JOURNAL OF GEOPHYSICAL RESEARCH, VOL. 98, NO. D2, PAGES 3023–3029, FEBRUARY 20, 1993

The Effect of Roughness Elements on Wind Erosion Threshold

M. R. RAUPACH

CSIRO Centre for Environmental Mechanics, Canberra, Australia

D. A. GILLETTE

Geophysical Laboratory for Climate Change, Air Resources Laboratory, NOAA, Boulder, Colorado

J. F. LEYS

Department of Conservation and Land Management, Buronga, New South Wales, Australia

A theory is developed to describe the dependence upon roughness density of the threshold friction velocity ratio R_t, the ratio of the threshold friction velocity of an erodible surface without roughness to that of the surface with nonerodible roughness present. The roughness density is quantified by the frontal area index λ. The prediction is $R_t = (1 - m\sigma\lambda)^{-1/2}(1 + m\beta\lambda)^{-1/2}$, where β is the ratio of the drag coefficient of an isolated roughness element on the surface to the drag coefficient of the substrate surface itself; σ is the basal-to-frontal area ratio of the roughness elements; and m (<1) is a parameter accounting for differences between the average substrate surface stress and the maximum stress on the surface at any one point. The prediction is well verified by four independent data sets.

1. INTRODUCTION

It is well known that the erosion of soil by wind is strongly attenuated by the presence of nonerodible roughness elements on the surface. The roughness elements can be of several kinds. Wind erosion suppression is achieved in conservation farming systems by retaining stubbles or crop residues on the ground during fallow periods. On suitable soils, erosion protection is provided by large "nonerodible" soil particles or aggregates, nominally greater than 0.85 mm in diameter [*Chepil*, 1951]. Protection in grazing or rangeland environments is aided by large roughness elements such as bushes, shrubs, or trees. The basic suppression mechanism is the same in each case: the roughness elements decrease the wind stress on the erodible surface by absorbing a significant fraction of the downward momentum flux from the airflow above.

There are two ways in which erosion suppression by roughness has been quantified. The first, older method is through the "soil flux ratio" $R_Q = Q_R/Q_S$, the ratio of the streamwise soil flux Q_R in the presence of roughness elements to the flux Q_S over a bare soil without roughness elements, exposed to the same wind conditions. The streamwise soil flux (units mass length^{-1} time^{-1}) is usually measured with a portable wind erosion tunnel. (In previous work, R_Q has often been called the "soil loss ratio," but this terminology is slightly inaccurate because soil loss is actually the streamwise derivative of soil flux.) *Fryrear* [1985] presented data on R_Q for various kinds of roughness over various soils, including both his own and earlier measurements [*Chepil*, 1944; *Siddoway et al.*, 1965; *Lyles and Allison*, 1981]. Similar data have also been presented by *Findlater et al.* [1990] and *Leys* [1991]. All these data are fitted fairly well by a simple exponential curve of the form $R_Q = \exp(-\alpha f_c)$ where f_c is the fraction of soil cover by the nonerodible roughness and $\alpha \approx 4 \pm 1$ is an empirical constant.

The second approach, introduced by *Gillette and Stockton* [1989] (henceforth called *GS*) is to quantify the effect of the roughness on the threshold friction velocity u_{*t}, through the "threshold friction velocity ratio" $R_t = u_{*tS}/u_{*tR}$. This is the ratio of u_{*t} for a bare soil surface (u_{*tS}) to that with roughness present (u_{*tR}). Like R_Q, R_t decreases from 1 as roughness is added to an initially bare erodible surface. The use of threshold friction velocity to quantify roughness effects is based on the hypothesis that the main dynamical effect of adding roughness to an erodible surface is to increase u_{*t}. Its main conceptual advantage is a relationship to the dynamics of drag partition on a rough surface.

The purpose of this paper is to present an analysis of the effect of roughness on the second of these parameters, the threshold friction velocity ratio R_t, using a general treatment of drag and drag partition on rough surfaces developed in a previous paper [*Raupach*, 1992]. We first discuss drag partition in section 2. A theoretical prediction for the dependence of R_t on the amount of roughness present is derived in section 3 and tested against data in section 4. Discussion and conclusions appear sequentially in section 5.

It is necessary to quantify the "amount of roughness present." The attenuating effect of roughness on erosion is closely related to momentum absorption by roughness, which is controlled primarily by the total frontal area (projected area from the mean wind direction) of the roughness elements on unit ground area [*Marshall*, 1971; *Wooding et al.*, 1973]. Hence the most appropriate measure is the frontal area index or roughness density λ defined by

$$\lambda = nbh/S \tag{1}$$

where ground area S is occupied by n roughness elements, each with mean breadth b, mean height h, and mean frontal area bh. A second roughness measure, used agronomically

Paper number 92JD01922.

for stubble or crop residue, is the mass M of residue per unit area, which can be assumed to be linearly related to λ with a proportionality coefficient dependent on the stubble type. A third measure, widely used in previous work [e.g., *Fryrear*, 1985; *Findlater et al.*, 1990] is the fraction f_c of soil covered when viewed from above; if the roughness is uniformly distributed and isotropically oriented, then f_c is related to λ by $f_c = 1 - e^{-\lambda}$. A similar exponential relationship between f_c and M has been given by *Gregory* [1982]. A fourth kind of roughness measure is the aerodynamic roughness length z_0 appearing in the logarithmic velocity profile law; relationships between z_0 and λ are discussed extensively by *Wooding et al.* [1973] and *Raupach* [1992], for instance.

2. Stress Partition

An advantage of the threshold friction velocity approach is its relationship to the dynamics of shear stress (drag) partition on a rough surface. The total force F acting on area S of a rough surface (where S is large enough to contain many roughness elements) can be split into a part F_R acting on the roughness elements and a part F_S acting on the substrate surface, such that $F = F_R + F_S$. Likewise, the total surface stress $\tau = F/S$ can be split into components $\tau_R = F_R/S$ and $\tau_S = F_S/S$ acting on the roughness elements and substrate surface, respectively:

$$\tau = \rho u_*^2 = \tau_R + \tau_S \tag{2}$$

where ρ is the air density and u_*^2 the friction velocity. In (2), τ_S is normalized over the total ground area S rather than the exposed (erodible) ground area S'. The difference $S - S'$ is the total basal area of the roughness elements on area S. The drag force per unit exposed ground area, τ'_S, is given by

$$\tau'_S = (S/S')\tau_S = \frac{\tau_S}{1 - \sigma\lambda} \tag{3}$$

where σ is the ratio of roughness-element basal area to frontal area, so that $\sigma\lambda = 1 - S'/S$ is the basal area index (the basal area per unit ground area). The roughness element geometry determines σ; for instance,

$$\sigma = \frac{\pi b}{4h} \text{ (vertical axis cylinders)}$$
$$\sigma = 2 \text{ (hemispheres)} \tag{4}$$

where h is cylinder height and b diameter. In terms of τ'_S, (2) becomes

$$\tau = \tau_R + (1 - \sigma\lambda)\tau'_S \tag{5}$$

The stress partition between the roughness elements and the substrate surface is specified fully by any of the ratios τ_R/τ, τ_S/τ, or τ'_S/τ. The "stress partition problem" can be stated as finding the dependence of these ratios on λ and the roughness element shape. The ratios are determined in the limits of low and high λ by

$$\tau_R/\tau \to 0,\ \tau_S/\tau \to 1 \text{ as } \lambda \to 0$$
$$\tau_R/\tau \to 1,\ \tau_S/\tau \to 0 \text{ as } \lambda \to \infty \tag{6}$$

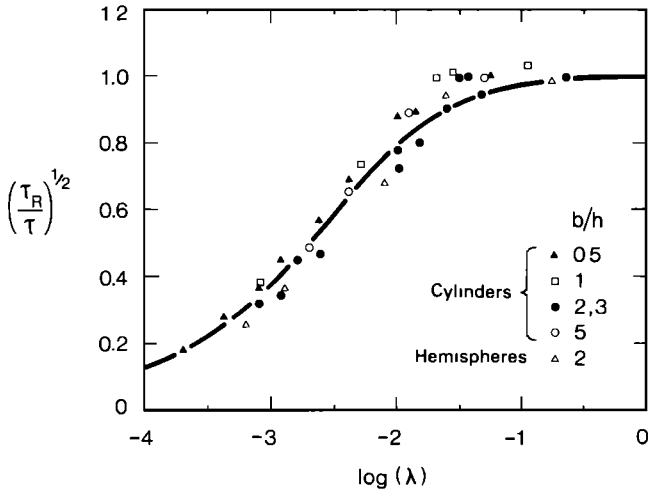

Fig. 1. Prediction of (7) for stress partition, with $C_R = 0.3$ and $C_S = 0.0018$, compared with data of *Marshall* [1971]. Ordinate is Marshall's stress partition parameter, $(\tau_R/\tau)^{1/2}$. Data are for cylinders with $b/h = 0.5$, 1, 2, 3, and 5 and hemispheres ($b/h = 2$).

from the physical requirement that the roughness accounts for negligible stress when λ is small and all the stress when λ is large.

Marshall [1971] studied stress partition experimentally in a wind tunnel, by measuring τ and τ_R independently for several kinds of roughness element over a wide range of λ. A drag balance and momentum integral methods were used to find τ, while τ_R was obtained by mounting individual elements on a miniature force balance. Figure 1 plots Marshall's data as $\sqrt{\tau_R/\tau}$ against log (λ), a form suggested by his colleagues Wooding and Bradley [*Wooding et al.*, 1973]. The data show that essentially all the stress is absorbed by the elements ($\tau_R/\tau \approx 1$) for λ greater than about 0.03, while the stress contribution due to the elements is negligible only when λ is less than about 0.003. Also, there is only a weak experimental dependence of stress partition on roughness element shape and the arrangement of elements on the surface. Therefore these factors can be neglected to a good approximation, leaving λ as the sole roughness parameter specifying stress partition.

An indication of the overall quality of Marshall's data is provided at high λ, for which the stress on the substrate is expected to become negligible so that $\tau_R \to \tau$. The independent measurements of τ_R and τ satisfy this constraint to within a few percent (Figure 1), suggesting that the measurements are internally consistent to a remarkably high accuracy.

An effort to describe Marshall's data theoretically was made by *Wooding et al.* [1973], who proposed, from arguments based on the logarithmic law of the wall for fluid mean velocity, that $(\tau_R/\tau)^{1/2}$ is linear in ln (1/λ) and therefore in ln (λ): $(\tau_R/\tau)^{1/2} = a_1 \ln(\lambda) + a_2$, where a_1 and a_2 are empirical constants. This suggestion motivated the choice of axes in Figure 1. With appropriate constants this form approximately agrees with the data in the middle part of the λ range in Figure 1, but it cannot be correct at either low or high λ as it does not satisfy (6) in either limit.

An alternative analysis of stress partition is provided in a companion to the present paper [*Raupach*, 1992]. The basic hypotheses are (1) that the surface stress deficit behind an

isolated roughness element can be described by an "effective shelter area" which can be dimensionally characterized by element geometry and bulk flow properties and (2) the interaction of elements is such that effective shelter areas are randomly superimposed. The theory leads to the stress partition predictions

$$\frac{\tau_R}{\tau} = \frac{\beta\lambda}{1+\beta\lambda}$$

$$\frac{\tau_S}{\tau} = \left(1 - \frac{\tau_R}{\tau}\right) = \frac{1}{1+\beta\lambda} \tag{7}$$

$$\frac{\tau'_S}{\tau} = \left(\frac{1}{1-\sigma\lambda}\right)\left(1 - \frac{\tau_R}{\tau}\right) = \frac{1}{(1-\sigma\lambda)(1+\beta\lambda)}$$

where $\beta = C_R/C_S$ is the ratio of element to surface drag coefficients. Here C_R is the drag coefficient for an isolated roughness element mounted on the surface (as distinct from the drag coefficient for the same element in a uniform free stream) and C_S is the drag coefficient for the ground surface in the absence of roughness. These coefficients are defined by

$$\tau_S(\lambda = 0) = \rho C_S U_h^2$$

$$\Phi = \rho C_R b h U_h^2 \tag{8}$$

where $\tau_S(\lambda = 0)$ is the stress on the unobstructed ground surface with no roughness present; Φ is the drag force on an isolated, surface-mounted roughness element; and U_h is the mean wind velocity at the height h of the roughness elements. Note the omission of the factor 1/2 which is often included in (8). Both C_R and C_S are independently measurable quantities in principle, so the stress partition prediction, (7), has no arbitrary constants. Also, (7) satisfies the limits in (6).

Data on C_R for several shapes of roughness element were reviewed by *Taylor* [1988]. He found that there is some experimental uncertainty in C_R, especially for smooth shapes such as hemispheres where separation points are not geometrically determined, leading to a dependence of C_R on Reynolds number hU_h/ν, where ν is the kinematic viscosity of air. From the data in the work of *Taylor* [1988] and other evidence, *Raupach* [1992] suggested $C_R \approx 0.3 \pm 25\%$ for cubic, cylindrical, and hemispheric roughness elements at Reynolds numbers between about 10^3 and 5×10^4, the relevant range for Marshall's experiment.

Values for C_S can be deduced from the law of the wall for a smooth surface, $U(z)/u_* = \kappa^{-1} \ln (zu_*/\nu) + B$, where $U(z)$ is the mean velocity at height z, $\kappa \approx 0.4$ (the von Karman constant), and $B \approx 5$. One finds that to within about 10%, $C_S \approx 0.0018$ for Marshall's experiment.

The curve in Figure 1 is (7) with $\beta = C_R/C_S = 0.3/0.0018 \approx 170$. The prediction fits the data very well except for a very small discrepancy near $\lambda \approx 0.03$, where the data reach $\sqrt{\tau_R/\tau} \approx 1$ at slightly lower λ values than the prediction. Since a few of the measured τ_R/τ values slightly exceed 1, which is physically implausible, it is possible that this discrepancy is caused by small measurement errors (of the order of a few percent) leading to slight overestimation of τ_R/τ. Given that the measurements of τ_R and τ were by independent methods, such small errors are likely, despite the overall internal consistency of the data set. We therefore take Figure 1 as evidence that (7) adequately describes stress partition.

3. Threshold Friction Velocity Ratio: Theory

At erosion threshold on a surface protected by nonerodible roughness elements, the overall stress is, by definition,

$$\tau = \rho u_{*tR}^2 \tag{9}$$

where u_{*tR} is the threshold friction velocity with roughness present. *GS* proposed that under identical (erosion threshold) conditions the average stress on the exposed surface is equal to the stress required to initiate erosion on a bare erodible surface with no roughness elements present:

$$\tau'_S = \rho u_{*tS}^2 \tag{10}$$

Taking the ratio of (10) and (9) and using (7) to specify the stress partition, we obtain

$$R_t = \frac{u_{*tS}}{u_{*tR}} = \left(\frac{\tau'_S}{\tau}\right)^{1/2} = \left[\frac{1}{(1-\sigma\lambda)(1+\beta\lambda)}\right]^{1/2} \tag{11}$$

This is our basic prediction for R_t. The factor $(1 + \beta\lambda)^{-1/2}$ accounts for the reduction of surface stress by shelter from the nonerodible elements; the factor $(1 - \sigma\lambda)^{-1/2}$ accounts for the "amplification" of the stress τ'_S on the erodible surface over the difference $\tau - \tau_R$ between the total stress and the stress acting on the roughness elements, caused by the occupation of a fraction $\sigma\lambda$ of the total surface area by the bases of roughness elements.

The prediction can be extended a little to account for a possible weakness in (10): the threshold of particle movement is determined not by the spatially averaged stress on the exposed surface, τ'_S, but by the largest stress acting at any point of the surface, say τ''_S. The value of τ''_S depends not only on the mean surface stress τ'_S but also on the behavior of the spatial surface stress distribution at its high tail. Spatially nonuniform erosion patterns around nonerodible roughness elements on erodible beds are well documented by *Iversen et al.* [1991]. Hence (10) and (11) should be replaced by

$$\tau''_S = \rho u_{*tS}^2, \quad R_t = \frac{u_{*tS}}{u_{*tR}} = \left(\frac{\tau''_S}{\tau_R}\right)^{1/2} \tag{12}$$

because the erodible substrate stress ρu_{*tS}^2 is equal to τ''_S rather than τ'_S at erosion threshold.

The ranking of the four stresses τ, τ_S, τ'_S, and τ''_S is constrained because nonuniformity in the surface stress distribution always causes τ''_S to exceed τ'_S. A second (but more speculative) constraint is that the maximum stress on the ground surface at any point is unlikely to exceed the total stress τ. These constraints yield the ranking

$$\tau_S < \tau'_S < \tau''_S < \tau \tag{13}$$

(surface stress averaged over total area < surface stress averaged over exposed area < maximum surface stress on exposed area < total stress.)

Beyond the ranking (13) it is difficult to analyze precisely the relationship between τ''_S and λ, although such a relationship is provided for the other stresses by (7). Analysis of τ''_S

requires one to know or assume details of the spatial distribution of surface stresses around roughness elements, a level of detail which was deliberately avoided in the theory of *Raupach* [1992]. Therefore (partly guided by data presented below) we make the empirical assumption that τ''_S for a particular rough surface is equal to τ'_S for a less dense (lower λ) rough surface composed of the same roughness elements:

$$\tau''_S(\lambda) = \tau'_S(m\lambda) \tag{14}$$

where m is a constant ≤ 1, which accounts for the difference between τ''_S and τ'_S. Although empirically based, (14) is simple, plausible, and conforms with (13).

Combining (7), (9), (12), and (14) gives

$$R_t = \left(\frac{\tau''_S}{\tau}\right)^{1/2} = \left[\frac{1}{(1 - m\sigma\lambda)(1 + m\beta\lambda)}\right]^{1/2} \tag{15}$$

which generalizes (11) to account for nonuniformity of the surface stress, the extent of which is described by the parameter m (≤ 1). Equations (11) and (15) are identical when $m = 1$. The main quantitative difference between the two is due to the appearance of m in the factor $(1 + m\beta\lambda)^{-1/2}$; the presence of m in the other factor, $(1 - m\sigma\lambda)^{-1/2}$, usually has a far smaller effect because the situations of practical interest occur when $\lambda \ll 1$, and typically $\sigma \sim 1$, whereas $\beta \sim 100$. Hence, in practice, the main effect of nonuniformity in the surface stress is to replace $\beta = C_R/C_S$ in (11) with $m\beta = mC_R/C_S$.

In section 4 the prediction of (15) for $R_t(\lambda)$ is compared with direct measurements from four different experiments.

4. Threshold Friction Velocity Ratio: Comparisons With Data

4.1. *Data of Gillette and Stockton [1989]*

GS measured $R_t = u_{*tS}/u_{*tR}$ in a small wind tunnel, using mixtures of small, erodible spheres and larger, nonerodible spheres which were half buried in the flat erodible bed, giving hemispheric nonerodible elements. Friction velocities were measured by applying a wake law to mean velocity data in the turbulent boundary layer, while (fluid) threshold friction velocities were identified by using a particle impact sensor to determine the onset of particle movement with increasing wind velocity. Three erodible sphere diameters (0.107, 0.250, and 0.575 mm) and three nonerodible diameters (2.4, 4.2, and 11.2 mm) were used; no strong systematic trends with either diameter were evident. Figure 2 shows all data for R_t as a function of λ, the roughness density of nonerodible hemispheres. The *Marshall* [1971] stress partition data are included for comparison, in the form $(\tau'_S/\tau)^{1/2} = (1 - \tau_R/\tau)^{1/2}(1 - \sigma\lambda)^{-1/2}$ required by (11). Predictions from (11) and (15) are also shown.

Equation (11) (or (15) with $m = 1$) agrees well with the Marshall data when $\beta = 170$ and $\sigma = 2$ (the value for hemispheres). This is expected because this value of β produces a good fit to the same data in Figure 1. A few points near $(\tau'_S/\tau)^{1/2} = 0$ lie somewhat off the prediction, but representation of these data in the form $(\tau'_S/\tau)^{1/2}$ greatly magnifies very small measurement errors in τ_R or τ when both quantities are nearly equal, so the points near $(\tau'_S/\tau)^{1/2} = 0$ have a very high standard error, of the order of tens of

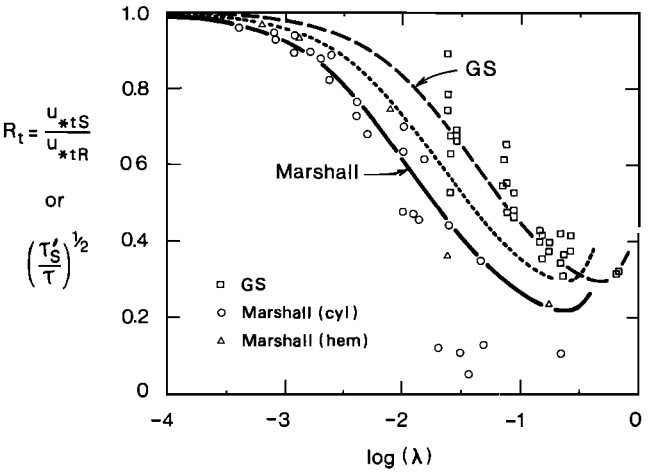

Fig. 2. Data for threshold friction velocity ratio, $R_t = u_{*tS}/u_{*tR}$ [*Gillette and Stockton*, 1989 (*GS*)] and stress partition ratio $(\tau'_S/\tau)^{1/2}$ [*Marshall*, 1971] plotted against log (λ). Curves are (15) with (β, σ, m) = (170, 2, 1) (solid); (90, 2, 1) (dotted); and (90, 2, 0.5) (dashed).

percent, and do not indicate serious disagreement between the data and the $\beta = 170$ curve.

For the *GS* experiment, an independent estimate of $\beta = C_R/C_S$ is 0.3/0.0033 = 90. The value $C_R = 0.3$ for hemispheres is retained from the Marshall data, while $C_S = 0.0033$ is estimated from the law of the wall for a smooth surface. Use of the smooth wall law is justified because the substrate surface in the *GS* experiment was dynamically smooth despite the presence of small erodible spheres; the Reynolds number du_{*tS}/ν was about 15 (d being erodible sphere diameter), in comparison with the value of about 70 required to establish rough-wall flow.

The prediction of (15) with $\beta = 90$, $\sigma = 2$, and $m = 1$, shown in Figure 2, does not agree with the *GS* data; it lies about half way between the Marshall and the *GS* data sets. To obtain agreement between (15) and *GS* data using the independent estimate $\beta = 90$, the parameter m must be less than 1. A prediction with $\beta = 90$, $\sigma = 2$, and $m = 0.5$, which fits the *GS* data well, is also shown in Figure 2. This suggests that there is indeed a significant difference between the maximum surface stress τ''_S, which initiates particle movement, and the average surface stress τ'_S measured by *Marshall* [1971].

With these data it is also possible to examine the role played by roughness-element basal areas in modifying R_t. This appears in the predictions through the factor $(1 - \sigma\lambda)^{-1/2}$ in (11), which "amplifies" τ'_S over τ_S. This amplification increases as λ increases, to the extent that (11) and (15) both predict that the function $R_t(\lambda)$ has a minimum, beyond which R_t increases with increasing λ. Figure 3 shows the effect of varying σ (the roughness-element basal-to-frontal area ratio) upon the prediction of (15) for the *GS* data. Three curves are shown, with $\sigma = 0$, 1, and 2 (with 2 being the correct value for the hemispheres used by *GS*), and with $\beta = 90$ and $m = 0.5$, as for the *GS* curve in Figure 2. The predicted curve from Figure 2 for the Marshall data is also included for comparison. At high λ the *GS* data are not consistent with predictions using spuriously low values of σ (0 and 1); rather, the measured R_t values vary very slowly with λ when λ is above about 0.1, as predicted by (15) with

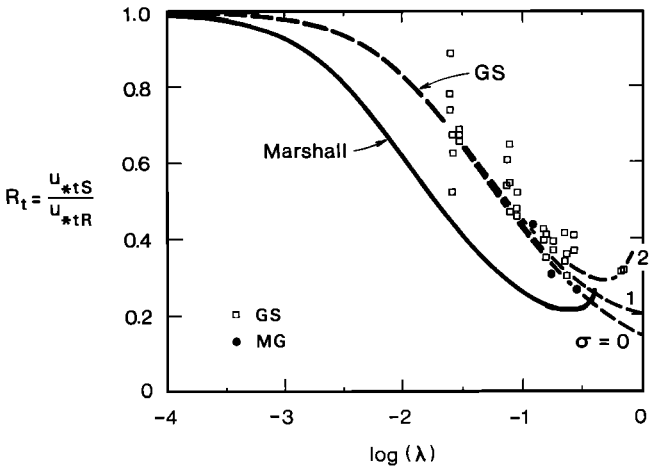

Fig. 3. Effect of σ on prediction of (15). Curves are (15) with (β, σ, m) = (90, 2, 0.5); (90, 1, 0.5); and (90, 0. 0.5). Threshold friction velocity data from *GS* and *Musick and Gillette* [1990] (*MG*). Locus of *Marshall* [1971] data is shown by prediction from (15), as in Figure 2.

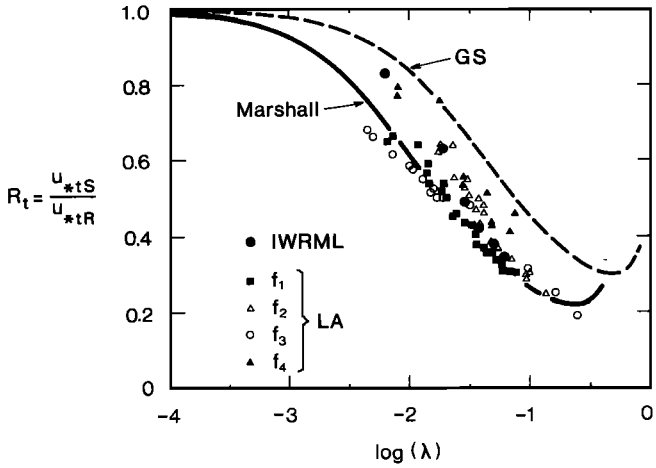

Fig. 4. Data of *Iversen et al.* [1991] (*IWRML*) and *Lyles and Allison* [1975] (*LA*) for threshold friction velocity ratio $R_t = u_{*tS}/u_{*tR}$ plotted against log (λ). Data sets f_1, f_2, f_3, and f_4 correspond to Figures 1 to 4 in the work of *LA* and have the following values of element density n/S (m^{-2}) and cylinder diameter b (mm): (f_1, 387, 6.6); (f_2, 387, 15.9); (f_3, 97, 6.6); and (f_4, 24, 6.6 and 11, 15.9). Curves are (15) with (β, σ, m) = (170, 2, 1) (solid, representing Marshall data) and (90, 2, 0.5) (dashed, representing *GS* data).

the correct value $\sigma = 2$. This indicates that the inclusion of σ in (15) improves the predictions, perhaps up to λ values near the point of the minimum in $R_t(\lambda)$. Beyond this point, (15) should not be considered as reliable because the denominator becomes the product of very small and very large terms, neither of which is sufficiently well constrained in the limit $\lambda \to \infty$ for their product to be well constrained. However, at these large λ values, shelter is very effective and the determination of R_t is not usually a practical problem.

4.2. *Field Data: Musick and Gillette [1990]*

Musick and Gillette [1990], henceforth *MG*, presented three values R_t obtained over erodible shrub-vegetated field sites in the United States and the former USSR. These data are included in Figure 3. They are consistent with the *GS* data. It is not possible to establish independent values for C_R and C_S, but one would expect both C_R and C_S to be larger in the field than for the *GS* experiment: C_R because of the high drag of a porous shrub relative to a smooth hemisphere and C_S because the ground is unlikely to be aerodynamically smooth. Also, one would expect σ for a shrub to be a good deal smaller than 1 (in comparison with the value 2 for a hemisphere). It is therefore plausible to model the *MG* field data with β and m similar to the *GS* values with σ smaller then the *GS* value. Figure 3 shows that the *MG* data are consistent with this choice of parameters. In particular, the *MG* data support the finding, from the above analysis of the *GS* data, that the parameter m in (15) is substantially less than 1, so that there is a significant difference between the maximum surface stress τ''_S, which initiates erosion, and the average surface stress τ'_S on the erodible surface.

4.3. *Quasi-Stable Beds: Lyles and Allison [1975] and Iversen et al. [1991]*

Lyles and Allison [1975], henceforth *LA*, presented extensive wind tunnel measurements of R_t, using sand (0.15 to 0.59 mm) as the erodible material and arrays of vertical axis cylinders as the nonerodible elements. Measurement of u_* was by use of the logarithmic profile law for mean velocity, with threshold friction velocities determined as the values of u_* at a preset, very small streamwise sand flux. This technique would yield impact, rather than fluid, threshold friction velocities. Variation of λ was achieved by allowing the exposed cylinder height above the erodible bed to increase naturally through the course of the experiment as sand was eroded from array. This meant that the erodible surface was not flat, as in the *GS* experiment, but instead was configured into a quasi-stable bed topography with a scour region in front of and a deposition region behind each element. Four array configurations were tested.

A similar experiment was performed by *Iversen et al.* [1991], henceforth *IWRML*. They used arrays of rectangular wooden blocks as nonerodible elements, with variation of λ produced by the same natural sand removal method as *LA*. They documented the quasi-stable bed forms around the elements with photographs.

Figure 4 shows the *LA* and *IWRML* data sets, which share the common feature of a quasi-stable bed topography rather than the flat bed by *GS*. The general positions of the *Marshall* [1971] and *GS* data sets are indicated by their predicted curves from (15) (as in Figure 2). Although there is some scatter between the various experiments, the trend is for the *LA* and *IWRML* data to fall mainly near the Marshall data rather than the *GS* data. There is a disagreement, amounting to a displacement of a factor of 2 to 4 in λ, between the *GS* data and the grouped *LA-IWRML* data.

Several factors are likely to contribute to this experimental difference. Obvious differences in experimental arrangement include (1) cylindrical (*LA*) or rectangular (*IWRML*) roughness elements, as opposed to the hemispheric elements used by *GS*; (2) the use of sand (*LA* and *IWRML*) as opposed to glass beads (*GS*) as the erodible material; (3) different techniques for measuring friction velocities; (4) the use of fluid and impact threshold friction velocities by *GS*

and *LA*, respectively; (5) different sizes of wind tunnel; and (6) the different bed topographies noted above.

Of these, difference 1 is unlikely to be important because the differences in stress partition for hemispheres and cylinders are not large according to the *Marshall* [1971] data. Also, at least the low-λ data in the *GS*, *LA*, and *IWRML* experiment sets are all for similar roughness-element densities, heights, and breadths. Difference 2 is not significant because the threshold erosion properties of sand and glass beads are quite similar in the absence of roughness. Regarding differences 3 and 5, there is no direct evidence of problems in any of the three experiments from either stress measurement techniques or tunnel size; the latter was carefully considered by *Owen and Gillette* [1985]. Difference 4, between fluid and impact threshold friction velocities, is unlikely to be significant because the comparison is between ratios of the threshold friction velocities: fluid to fluid for *GS* and impact to impact for *LA*. Thus the difference between the threshold measures should be largely removed by normalization.

We conclude that the likely major cause of the difference is difference 6, the bed topography. The likely effect of scouring and stabilization of the erodible surface is to increase u_{*tR} relative to that observed over a flat bed. Equilibration of the bed involves minimization of spatial stress gradients at the surface, since these gradients induce differential horizontal sand fluxes and therefore change the topography. Therefore it is reasonable to suppose that $m \approx 1$ for a stabilized bed. This is broadly confirmed by Figure 4, in which the average of the *LA* and *IWRML* data is fairly close to the Marshall prediction, for which $m = 1$.

5. Discussion and Conclusions

The theory outlined here involves two key simplifications. First, we describe surfaces only in terms of the roughness density λ, without accounting for roughness element shape differences. This is motivated by the experimental results of *Marshall* [1971], which show that stress partition is influenced primarily by λ and only secondarily by element shape, so that a description in terms of λ alone is a reasonable approximation.

Second, the present theory avoids direct consideration of the nature of the turbulence close to the surface. For instance, we have not considered the nature of the turbulent events responsible for mobilizing particles from the erodible surface at erosion threshold. Over both smooth and rough surfaces these events can be identified with gusts, or occurrences of high streamwise velocities close to the substrate surface and therefore high stress on the substrate. Because of the fluctuating nature of the instantaneous substrate stress, the instantaneous stress required to detach a particle from the erodible bed substantially exceeds the average threshold stress ρu_{*tS}^2, by a factor dependent on the probability density function $p(\tau)$ for substrate stress (or the equivalent function for horizontal wind speed very close to the substrate). It is expected that $p(\tau)$ changes as roughness is added to an erodible surface, because turbulence within a roughness canopy tends to be non-Gaussian, intermittent, and dominated by gusts, in the sense that the skewness for streamwise velocity is large and positive; all these properties are accentuated as roughness density increases [e.g., *Raupach et al.*, 1991]. Therefore one expects particles to be mobilized somewhat more easily over a roughened erodible surface than a smooth surface, given the same average stress on the substrate in each case. At the level of description adopted here, such effects must be regarded as among those determining the parameter m in (14).

It is of interest to compare the present work with a recent suggestion by *IWRML* for rationalizing $R_t(\lambda)$ data from different experiments. They found a closer collapse of the *GS*, *LA*, and their own data by plotting R_t against $C_R\lambda$ rather than λ. The present work provides some justification for this, in that (15) predicts $R_t = (C_S/C_R\lambda)^{1/2}$ for the simple case $\sigma = 0$, $m = 1$, and $C_S \ll C_R\lambda$. If variations in C_S are also discounted, one obtains $R_t \sim (C_R\lambda)^{-1/2}$. Averaged over three data sets, *IWRML* found $R_t \sim (C_R\lambda)^{-0.35}$. This suggests that the above simplifications are qualitatively indicative but a little too severe for quantitative work. The quality of the data collapse obtained by *IWRML* may also have an influenced by their use of free-stream drag coefficients to determine C_R, rather than the more appropriate drag coefficients for surface-mounted obstacles.

Our basic conclusion is that (15) provides an adequate description of the threshold friction velocity ratio R_t, rationalizing the difference between the Marshall stress partition data and both the *GS* (laboratory) and the *MG* (field) data for R_t. Two factors contribute about equally to the difference: different values of the drag coefficient ratio β and the fact that R_t is related to the maximum stress τ''_S on the exposed surface rather than the average stress τ'_S, the quantity determined by stress partition arguments. The latter effect is quantified through an empirical constant m, defined such that $\tau''_S(\lambda) = \tau'_S(m\lambda)$. It is found from comparisons of the Marshall and *GS* data that $m \approx 0.5$ for an approximately flat erodible surface. On the other hand, for an erodible surface which is contoured by wind into a quasi-stable, equilibrium bed topography, it is likely that m is close to 1. This is broadly supported by the experimental results of *LA* and *IWRML*.

For field application of (15), $R_t = u_{*tS}/u_{*tR} = (1 - m\sigma\lambda)^{-1/2}(1 + m\beta\lambda)^{-1/2}$, to determine the threshold friction velocity ratio R_t from the roughness density λ and the basal/frontal area ratio σ of the roughness elements, we tentatively recommend the approximate values $\beta = 100$, with $m = 0.5$ for flat erodible surfaces and $m = 1$ for surfaces which have been topographically stabilized by erosion.

References

Chepil, W. S., Utilization of crop residues for wind erosion control, *Sci. Agric.*, *24*, 307–319, 1944.

Chepil, W. S., Properties of soil which influence wind erosion, IV, State of dry aggregate structure, *Soil Sci.*, *72*, 387–401, 1951.

Findlater, P. A., D. J. Carter, and W. D. Scott, A model to predict the effects of prostrate ground cover on wind erosion, *Aust. J. Soil Res.*, *28*, 609–622, 1990.

Fryrear, D. W., Soil cover and wind erosion, *Trans. ASAE*, *28*, 781–784, 1985.

Gillette, D. A., and P. H. Stockton, The effect of nonerodible particles on wind erosion at erodible surfaces, *J. Geophys. Res.*, *94*, 12,885–12,893, 1989.

Gregory, J. M., Soil cover prediction with various amounts and types of crop residue, *Trans. ASAE*, *25*, 1333–1337, 1982.

Iversen, J. D., W. P. Wang, K. R. Rasmussen, H. E. Mikkelsen, and R. N. Leach, Roughness element effect on local and universal saltation transport, *Acta Mech., Suppl.*, *2*, 65–75, 1991.

Leys, J. F., The threshold friction velocities and soil flux rates of

selected soils in south-west New South Wales, Australia, *Acta Mech., Suppl., 2*, 103–112, 1991.

Lyles, L., and B. E. Allison, Wind erosion: Uniformly spacing nonerodible elements eliminates effects of wind direction variability, *J. Soil Water Conserv., 30*, 225–226, 1975.

Lyles, L., and B. E. Allison, Equivalent wind erosion protection from selected crop residues, *Trans. ASAE, 24*, 405–408, 1981.

Marshall, J. K., Drag measurements in roughness arrays of varying density and distribution, *Agric. Meteorol., 8*, 269–292, 1971.

Musick, H. B., and D. A. Gillette, Field evaluation of relationships between a vegetation structural parameter and sheltering against wind erosion, *Land Degradation Rehabil., 2*, 87–94, 1990.

Owen, P. R., and D. A. Gillette, Wind tunnel constraint on saltation, in *Proceedings of the International Workshop on the Physics of Blown Sand*, edited by O. E. Barndorff-Nielsen, pp. 253–269, University of Aarhus, Aarhus, Denmark, May 1985.

Raupach, M. R., Drag and drag partition on rough surfaces, *Boundary Layer Meteorol., 60*, 375–395, 1992.

Raupach, M. R., R. A. Antonia, and S. Rajagopalan, Rough-wall turbulent boundary layers, *Appl. Mech. Rec., 44*, 1–25, 1991.

Siddoway, F. H., W. S. Chepil, and D. V. Armbrust, Effect of kind, amount and placement of residue on wind erosion control, *Trans. ASAE, 8*, 327–331, 1965.

Taylor, P. A., Turbulent wakes in the atmospheric boundary layer, in *Flow and Transport in the Natural Environment: Advances and Applications*, edited by W. L. Steffen and O. T. Denmead, pp. 270–292, Springer-Verlag, New York, 1988.

Wooding, R. A., E. F. Bradley, and J. K. Marshall, Drag due to regular arrays of roughness elements of varying geometry, *Boundary Layer Meteorol., 5*, 285–308, 1973.

D. A. Gillette, Geophysical Laboratory for Climate Change, Air Resources Laboratory, NOAA, Boulder, CO 80303.

J. F. Leys, Department of Conservation and Land Management, P.O. Box 7, Buronga, New South Wales 2648, Australia.

M. R. Raupach, CSIRO Centre for Environmental Mechanics, GPO Box 821, Canberra Mountain, Canberra ACT 2601, Australia.

(Received February 7, 1992;
revised August 13, 1992;
accepted August 13, 1992.)